



ELSEVIER

Atmospheric Research 79 (2006) 241–265

---

---

ATMOSPHERIC  
RESEARCH

---

---

www.elsevier.com/locate/atmos

# The solution of the vector radiative transfer equation using the discrete ordinates technique: Selected applications

V.V. Rozanov, A.A. Kokhanovsky\*

*Institute of Environmental Physics, Bremen University, Otto Hahn Allee 1, D-28334, Bremen, Germany*

Received 20 October 2004; accepted 12 June 2005

---

## Abstract

The paper is devoted to the presentation of a newly developed radiative transfer code SCIAPOL\_1.0 for a plane-parallel turbid slab illuminated by the monodirectional wide beam. The SCIAPOL\_1.0 is based on the discrete-ordinates solution of the vector radiative transfer equation.

The code is applied to a number of problems, including studies of the applicability of the scalar approximation for the calculation of light reflectance from aerosols, clouds, and molecular atmospheres. We also study the accuracy of the single scattering approximation as applied to the calculation of light reflection from molecular and cloudy atmospheres and propose new approximations for the calculation of the reflection function and the degree of light polarization under unpolarized light illumination conditions.

© 2005 Elsevier B.V. All rights reserved.

*Keywords:* Polarization; Radiative transfer; Clouds; Aerosols; Molecular scattering

---

## 1. Introduction

Light coming to the Earth from the Sun is unpolarized. However, it becomes polarized due to interaction with molecules and particles present in the terrestrial atmosphere. In particular, the theory of molecular scattering (Rayleigh, 1871) states that the polarization

---

\* Corresponding author. Tel.: +49 421 218 2915; fax: +49 421 218 4555.

*E-mail address:* alexk@iup.physik.uni-bremen.de (A.A. Kokhanovsky).

of initially unpolarized light after single scattering by a unit volume of air is almost 100% at right angles from the direction of incidence. Macroscopic particles like water droplets and ice crystals have smaller polarization ability at the scattering angle  $90^\circ$ . However, they also polarize light and can produce quite large values of the degree of polarization in some selected directions (e.g., around the scattering angle  $140^\circ$ , where the rainbow for water droplets is usually observed).

It is a well-known fact that calculations of scattered light intensity  $I$  (both in single and multiple light scattering regimes) cannot be done accurately without account for the polarization characteristics of a light beam (Rozenberg, 1955; Mishchenko et al., 1994; Lacis et al., 1998; Mishchenko, 2002). It means that the vector radiative transfer equation (VRTE) should be used whenever it is possible for studies of light transport in atmosphere and other turbid media. The use of the scalar radiative transfer equation (SRTE) could lead to large errors in many cases. Also the solution of the VRTE is of importance for remote sensing techniques (Hansen and Hovenier, 1974; Hansen and Travis, 1974; de Haan, 1987; Goloub et al., 2000; Mishchenko and Travis, 1997; Mishchenko et al., 2002; Kokhanovsky, 2003, 2004a). In particular, optical instruments are capable to measure not only  $I$  but also other components of the Stokes vector  $\vec{S}(I, Q, U, V)$  (Deschamps et al., 1994; Bovensmann et al., 1999). Spectral and angular measurements of  $\vec{S}$  bring us much more information on the medium under study as compared to just light intensity  $I$  (Kokhanovsky, 2003).

However, the usage of polarized light in astronomical applications, remote sensing and optical diagnostics of various turbid media is not widespread so far due to the complexity of the VRTE for the Stokes vector  $\vec{S}$ . The finding of the numerical solution of this integro-differential equation is a quite complex mathematical procedure (Hovenier, 1971; Siewert, 2000). Therefore, we have decided to develop a user-friendly web-based code for the solution of the VRTE. We hope that the code will be extensively used by the light scattering community for further advances in solutions of multiple direct and inverse transport problems.

The paper is organized as follows. In the next section, we briefly present the algorithm of the VRTE solution based on the discrete-ordinate technique (DOT) (Siewert, 2000). The superiority of this technique over the doubling–adding (de Haan, 1987) and Monte–Carlo (Tynes et al., 2001) is due to the weak dependence of the speed of computer simulations on the optical thickness of the medium under study in the framework of DOT. In the Section 3, we show the code performance solving a number of selected physical problems, including polarized light transport studies through molecular atmosphere, aerosols, and clouds. In particular, we consider the range of the validity of selected radiative transfer applications often used in applied studies.

## 2. The outline of the VRTE solution

The VRTE for a homogeneous isotropic symmetric plane-parallel light scattering slab is usually written as (Siewert, 2000):

$$\mu \frac{d\vec{S}(\tau, \mu, \phi)}{d\tau} = -\vec{S}(\tau, \mu, \phi) + \frac{\omega_0}{4\pi} \int_{-1}^1 d\mu' \int_0^{2\pi} d\phi' \hat{P}(\mu, \mu', \phi - \phi') \vec{S}(\tau, \mu', \phi') \quad (1)$$

for  $\tau \in [0, \tau_0]$ ,  $\mu \in [-1, 1]$  and  $\phi \in [0, 2\pi]$ . Here  $\tau_0$  is the optical thickness,  $\omega_0$  is the single scattering albedo,  $\hat{P}(\mu, \mu', \phi - \phi')$  is the phase matrix,  $\mu$  is the cosine of the polar angle  $\vartheta$  as measured from the positive  $\tau$ -axis and  $\phi$  is the azimuthal angle. The components of the Stokes vector  $\vec{S}$  are defined as follows (van de Hulst, 1980):  $I = I_l + I_r$ ,  $Q = I_l - I_r$ ,  $U = E_l E_r^* + E_r E_l^*$ ,  $V = i(E_l E_r^* - E_r E_l^*)$ , where we neglected a common multiplier and  $I_l = E_l E_l^*$  is the scattered light intensity in the meridional plane. This plane contains the normal to a light scattering slab and the direction of observation. The value of  $I_r = E_r E_r^*$  gives the scattered light intensity in the plane perpendicular to the meridional plane.  $E_l$  and  $E_r$  are components of the electric vector of the scattered wave defined relatively to the meridional plane in the same way as  $I_l, I_r$  (van de Hulst, 1980).

The value of  $\tau$  in Eq. (1) is the optical depth changing from 0 at the top of the turbid plane-parallel layer to the value  $\tau = \tau_0$  at the bottom. We will assume that there is a Lambertian surface with the spherical albedo  $A$  below a plane-parallel slab under study. The task is to find the vector  $\vec{S}$  at any point  $M$  with the radius-vector  $\vec{r}$  inside and outside of the scattering medium for arbitrary values of  $\omega_0, \tau_0$  and phase matrices  $\hat{P}(\mu, \mu', \phi - \phi')$ . It is assumed that the optical properties of the medium are the same at any point  $M(\vec{r})$  inside a slab. The slab is illuminated by a wide unidirectional light beam at the top ( $\tau = 0$ ). Both medium and light source are assumed to be time-independent and possible nonlinear and close-packed effects are neglected.

There are various approaches to solve the VRTE (Sobolev, 1956; Hovenier, 1971; de Haan, 1987; Siewert, 2000; Tynes et al., 2001; Ishimoto and Masuda, 2002). Among different approaches, we have selected for the numerical implementation the discrete ordinate technique as described by Siewert (2000). Full details are given by Siewert (2000). The main steps of the solution are outlined below.

*Step 1.* The phase matrix is presented in the form:

$$\hat{P}(\mu, \mu', \phi - \phi') = \frac{1}{2} \sum_{m=0}^L (2 - \delta_{0m}) \{ \langle \hat{A}^m(\mu, \mu') + \hat{D} \hat{A}^m(\mu, \mu') \hat{D} \rangle \cos(m(\phi - \phi')) + \langle \hat{A}^m(\mu, \mu') \hat{D} - \hat{D} \hat{A}^m(\mu, \mu') \rangle \sin(m(\phi - \phi')) \}. \tag{2}$$

where  $\hat{A}^m = \sum_{l=-m}^L \hat{P}_l^m(\mu) \hat{\Xi}_l \hat{P}_l^m(\mu')$ ,  $\hat{D} = \text{diag}\{1, 1, -1, -1\}$ ,  $\delta$  is the Kronecker symbol,  $L$  is the maximal order of Legendre polynomials used, and

$$\hat{\Xi}_l = \begin{pmatrix} \alpha_{1l} & \beta_{1l} & 0 & 0 \\ \beta_{1l} & \alpha_{2l} & 0 & 0 \\ 0 & 0 & \alpha_{3l} & \beta_{2l} \\ 0 & 0 & -\beta_{2l} & \alpha_{4l} \end{pmatrix}, \tag{3}$$

$$\hat{P}_l^m(\mu) = \begin{pmatrix} P_l^m(\mu) & 0 & 0 & 0 \\ 0 & -\frac{1}{2} i^m \langle P_{m,2}^l(\mu) + P_{m,-2}^l(\mu) \rangle & \frac{1}{2} i^m \langle P_{m,2}^l(\mu) - P_{m,-2}^l(\mu) \rangle & 0 \\ 0 & \frac{1}{2} i^m \langle P_{m,2}^l(\mu) - P_{m,-2}^l(\mu) \rangle & -\frac{1}{2} i^m \langle P_{m,2}^l(\mu) + P_{m,-2}^l(\mu) \rangle & 0 \\ 0 & 0 & 0 & P_l^m(\mu) \end{pmatrix} \tag{4}$$

with

$$P_l^m(\mu) = \sqrt{\frac{(l-m)!}{(l+m)!}} \{1-\mu^2\}^{\frac{m}{2}} \frac{d^m}{d\mu^m} P_l(\mu), \quad (5)$$

$$P_{m,n}^l(\mu) = \frac{(-1)^{l-m} i^{n-m}}{2^l (l-m)!} \sqrt{\frac{(l-m)!(l+n)!}{(l+m)!(l-n)!}} \{1-\mu\}^{\frac{m-n}{2}} \{1+\mu\}^{\frac{m+n}{2}} \frac{d^{l-n}}{d\mu^{l-n}} \\ \times \left[ \{1-\mu\}^{l-m} \{1+\mu\}^{l+m} \right]. \quad (6)$$

Here

$$P_l(\mu) = \frac{1}{2^l l!} \frac{d^l}{d\mu^l} (\mu^2 - 1)^l \quad (7)$$

are Legendre polynomials,  $P_l^m(\mu)$  are associated Legendre functions,  $P_{m,n}^l(\mu)$  are generalized spherical functions. The Greek constants  $\{\alpha_{1l}, \alpha_{2l}, \alpha_{3l}, \alpha_{4l}, \beta_{1l}, \beta_{2l}\}$  are determined by the local scattering law. For instance, it follows for the dipole scattering (de Rooij, 1985):

$$\alpha_{10} = 1, \alpha_{12} = \frac{1}{2}, \alpha_{22} = 3, \alpha_{41} = \frac{3}{2}, \beta_{12} = \sqrt{\frac{3}{2}} \quad (8)$$

with all other constants being equal to zero. The table of Greek constants for media composed of identical randomly oriented oblate spheroids with the aspect ratio 2, the size parameter 3 and the refractive index  $1.53-0.006i$  is given by Kuik et al. (1992). Correspondent constants can be easily obtained for monodispersed and polydispersed spherical particles as well. Then the Mie theory (Van de Hulst, 1957) can be used (see, e.g., the FORTRAN code *spher.f* located at <http://www.giss.nasa.gov/~crrim/brf>).

Although the representation (2) looks quite cumbersome, it allows to solve two important problems. First of all the phase matrix  $\hat{P}$  is represented now by discrete Greek symbols. These symbols can be used to find  $\hat{P}$  at any combination of  $\mu$ ,  $\mu'$ , and  $\varphi = \phi - \phi'$ . The algorithms of finding matrices  $\hat{P}_l^m(\mu)$  and  $\hat{\Xi}_l$  are well known and straightforward (de Rooij, 1985; Siewert, 1997; Mishchenko et al., 2002).

In particular, for calculations of generalized spherical functions in Eq. (4), we use Wigner functions  $d_{m,\pm 2}^l(\vartheta)$  (Mishchenko et al., 2002):

$$-\frac{1}{2} i^m \langle P_{m,2}^l(\mu) + P_{m,-2}^l(\mu) \rangle = -\frac{1}{2} (-1)^m \langle d_{m,2}^l(\vartheta) + d_{m,-2}^l(\vartheta) \rangle. \quad (9)$$

This allows to avoid calculations with complex functions and use stable and accurate algorithms to calculate Wigner functions as described by Mishchenko et al. (2002). We also use properties:

$$P_l^m(\mu) = \sqrt{\frac{(l+m)!}{(l-m)!}} d_{m,0}^l(\vartheta) \quad (10)$$

to calculate the associated Legendre function.

Greek symbols are determined by the Stokes matrix  $\hat{M}$  of a single scattering law. The  $4 \times 4$  matrix  $\hat{M}$  is defined with respect to the scattering plane holding directions of incident and scattered beams. Due to the symmetry of the media under consideration, elements of this matrix correspondent to upper-right and down-left  $2 \times 2$  sub-matrices vanish. Greek symbols can be calculated from the elements of the matrix  $\hat{M}$  using following equations (de Rooij, 1985):

$$\alpha_{1l} = \frac{2l+1}{2} \int_{-1}^1 dx P_l^{00}(x) M_{11}(x), \quad \alpha_{4l} = \frac{2l+1}{2} \int_{-1}^1 dx P_l^{00}(x) M_{44}(x), \quad (11)$$

$$\beta_{1l} = \frac{2l+1}{2} \int_{-1}^1 dx P_l^{02}(x) M_{12}(x), \quad \beta_{2l} = \frac{2l+1}{2} \int_{-1}^1 dx P_l^{02}(x) M_{34}(x), \quad (12)$$

and  $\alpha_{2l} = 1/2 \{v_l + \varsigma_l\}$ ,  $\alpha_{3l} = 1/2 \{v_l - \zeta_l\}$ , where  $P_l^{s,m}(x) = i^s \sqrt{(l+|s|)!/(l-|s|)!} P_{l,s,m}^l(x)$ ,

$$v_l = -\frac{2l+1}{2} \sqrt{\frac{(l-2)!}{(l+2)!}} \int_{-1}^1 dx P_l^{2,-2}(x) \{M_{22}(x) - M_{33}(x)\}, \quad (13)$$

$$\varsigma_l = -\frac{2l+1}{2} \sqrt{\frac{(l-2)!}{(l+2)!}} \int_{-1}^1 dx P_l^{2,-2}(x) \{M_{22}(x) - M_{33}(x)\}. \quad (14)$$

Step 2. The following Fourier expansion of the Stokes vector is used:

$$\vec{S} = \frac{1}{2} \sum_{m=0}^L \sum_{k=1}^2 \hat{\Phi}_k^m(\phi - \phi_0) \vec{S}_k^m(\tau, \mu) + \pi \delta(\mu - \mu_0) \delta(\phi - \phi_0) \vec{F} \exp(-\tau/\mu), \quad (15)$$

where  $\mu_0 = \cos \vartheta_0$ ,  $\vartheta_0$  is the solar zenith angle,  $\phi_0$  is the solar azimuth, and  $\delta(\zeta - \zeta_0)$  is the delta function. The second term explicitly accounts for the attenuated direct light ( $\vec{F}$  is the Stokes vector of the incident light flux) and (Siewert, 2000)

$$\hat{\Phi}_1^m(\phi) = (2 - \delta_{0m}) \text{diag}\{\cos m\phi, \cos m\phi, \sin m\phi, \sin m\phi\},$$

$$\hat{\Phi}_2^m(\phi) = (2 - \delta_{0m}) \text{diag}\{-\sin m\phi, -\sin m\phi, \cos m\phi, \cos m\phi\}.$$

Step 3. The substitution of Eqs. (2), (15) in Eq. (1) gives:

$$\mu \frac{d\vec{S}_k^m(\tau, \mu)}{d\tau} = -\vec{S}_k^m(\tau, \mu) + \frac{\omega_0}{2} \sum_{l=m}^L \hat{P}_l^m(\mu) \hat{\Xi}_l \int_{-1}^1 d\mu' \hat{P}_l^m(\mu') \vec{S}_k^m(\tau, \mu') + \vec{Q}_k^m(\tau, \mu), \quad (16)$$

where

$$\vec{Q}_k^m(\tau, \mu) = \frac{\omega_0}{2} \sum_{l=m}^L \hat{P}_l^m(\mu) \hat{\Xi}_l \hat{P}_l^m(\mu_0) \hat{D}_k \vec{F} \exp(-\tau/\mu_0), \quad (17)$$

where  $\hat{D}_1 = \text{diag}\{1, 1, 0, 0\}$ ,  $\hat{D}_2 = \text{diag}\{0, 0, 1, 1\}$ . It follows for the unpolarized incident light:  $\vec{F} = F_0(1, 0, 0, 0)^T$ , where  $\mu_0 F_0$  is equal to the incident light irradiance at the top of

the layer. This equation is much more simple to handle as compared to Eq. (1). In particular, the discrete ordinate technique can be used to solve this equation. Then integro-differential Eq. (16) is reduced to the following system of differential equations:

$$\pm \mu_\sigma \frac{d\vec{S}(\tau, \pm \mu_\sigma)}{d\tau} = -\vec{S}(\tau, \pm \mu_\sigma) + \frac{\omega_0}{2} \sum_{l=m}^L \hat{P}_l^m(\pm \mu_\sigma) \hat{\mathbf{E}}_l \sum_{\rho=1}^N w_\rho \vec{S}_{l,\rho}(\tau) + \vec{Q}(\tau, \pm \mu_\sigma), \tag{18}$$

where  $\sigma=1, 2, \dots, N$ ,  $N$  is the number of Gauss quadrature points,  $\vec{S}_{l,\rho}(\tau) = \hat{P}_l^m(\mu_\rho) \vec{S}(\tau, \mu_\rho) + \hat{P}_l^m(-\mu_\rho) \vec{S}(\tau, -\mu_\rho)$  and the Fourier indices are suppressed for the sake of simplicity. Gauss quadrature points  $\{\mu_\sigma\}$  and weights  $\{w_\rho\}$  in Eq. (18) are defined for the use on the integration interval  $[0, 1]$ . For unpolarized incident light illumination conditions, we have:  $k=1$ . We only consider this case in the paper. So the correspondent index in Eq. (18) is omitted.

*Step 4.* The system of differential equations (18) is solved using DOT as described by Siewert (2000). In particular, the solution of the homogeneous equation (with  $\vec{Q} = 0$  in Eq. (18)) is found as follows:

$$\vec{S}_\pm^h(\tau) = \vec{R}_\pm(\tau) + \vec{C}_\pm(\tau), \tag{19}$$

where

$$\vec{R}_\pm(\tau) = \Delta_\pm \sum_{j=1}^{J_R} \left[ \mathbf{A}_j \vec{\Phi}_\pm(v_j) \exp\left\{-\frac{\tau}{v_j}\right\} + \mathbf{B}_j \vec{\Phi}_\mp(v_j) \exp\left\{-\frac{\tau_0 - \tau}{v_j}\right\} \right], \tag{20}$$

$$\vec{C}_\pm(\tau) = \Delta_\pm \sum_{v=1}^2 \sum_{j=1}^{J_C} \left[ \mathbf{A}_j^{(v)} \vec{F}_\pm^{(v)}(\tau, v_j) + \mathbf{B}_j^{(v)} \vec{F}_\mp^{(v)}(\tau_0 - \tau, v_j) \right], \tag{21}$$

$$\begin{aligned} \vec{F}_\pm^{(1)}(v_j) &= \text{Re} \left\{ \vec{\Phi}_\pm(v_j) \exp\left\{-\frac{\tau}{v_j}\right\} \right\}, \quad \vec{F}_\pm^{(2)}(v_j) \\ &= \text{Im} \left\{ \vec{\Phi}_\pm(v_j) \exp\left\{-\frac{\tau}{v_j}\right\} \right\}, \end{aligned} \tag{22}$$

where  $\Delta_+ = \text{diag}\{1, 1, \dots, 1\}$ ,  $\Delta_- = \text{diag}\{\hat{D}, \hat{D}, \dots, \hat{D}\}$  are  $4N * 4N$  diagonal matrix,  $v_j$  is the collection of separation constants,  $J_R$  is the number of real eigenvalues,  $J_C$  is the number of complex eigenvalues. Vectors  $\vec{\Phi}_\pm(v_j)$  with appropriate exponential multipliers are elementary solutions of a homogeneous equation, which can be found after solution of the correspondent eigenvalue problem (see Appendix B).

The particular solution of inhomogeneous Eq. (18) is found using infinite medium Green function approach. Correspondent derivations are given by Siewert (2000) and the result is:

$$\begin{aligned} \vec{S}_\pm^p(\tau) &= \Delta_\pm \sum_{j=1}^{J_R} \left[ \mathbf{A}_j(\tau) \vec{\Phi}_\pm(v_j) + \mathbf{B}_j(\tau) \vec{\Phi}_\mp(v_j) \right] \\ &+ 2\Delta_\pm \text{Re} \sum_{j=1}^{J_C} \left[ \mathbf{A}_j(\tau) \vec{\Phi}_\pm(v_j) + \mathbf{B}_j(\tau) \vec{\Phi}_\mp(v_j) \right], \end{aligned} \tag{23}$$

where functions  $\mathbf{A}_j(\tau)$  and  $\mathbf{B}_j(\tau)$  are found after integration of the infinite medium Green function with the right hand side of Eq. (18).

The general solution of Eq. (18) can be found as a sum of a particular solution (Eq. (23)) and the general solution of homogeneous Eq. (18):

$$\vec{S}_{\pm}(\tau) = \vec{S}_{\pm}^h(\tau) + \vec{S}_{\pm}^p(\tau), \tag{24}$$

which includes  $8N$  unknown constants  $\mathbf{A}_j, \mathbf{B}_j, j=1, 2, \dots, 4N$ .

*Step 5.* To find constants  $\mathbf{A}_j, \mathbf{B}_j$ , boundary conditions must be applied. In particular, one should take into consideration that there is no diffused light coming to the top of a scattering layer and the diffused light from underneath of a scattering layer is just due to the light reflection from the Lambertian surface with the spherical albedo  $A$ . Boundary conditions in the notation as for the step 3 are (Siewert, 2000):  $\vec{S}_k^m(0, \mu) = \vec{O}$ ,

$$\vec{S}_k^m(\tau_0, -\mu_\sigma) = 2A\delta_{0m}\delta_{1k}\hat{I}\left\langle \mu_0\hat{D}\vec{F}\exp(-\tau_0/\mu_0) + \sum_{\rho=1}^N w_\rho\mu_\rho\vec{S}_k^m(\tau_0, \mu_\rho) \right\rangle, \tag{25}$$

where  $\vec{O}$  is the zero vector and  $\hat{I} = \text{diag}\{1, 0, 0, 0\}$ ,  $\sigma=1, 2, \dots, N$ . To find the required constants from the appropriate system of equations, we use the subroutines DGETRF and DGETRS from the LAPACK package (Anderson et al., 1995).

*Step 6.* To find solution not only for Gauss angles  $\mu_\sigma$  but for all possible angles, we have incorporated in the code a post-processing procedure as described by Siewert (2000).

We incorporated steps 1–6 outlined above in the code SCIAPOL\_1.0, which is freely available over INTERNET at [www.iup.physik.uni-bremen.de/~alexk](http://www.iup.physik.uni-bremen.de/~alexk). The code is capable to find the Stokes vector at any point  $\vec{r}$  and at any direction specified by angles  $(\vartheta, \varphi)$  inside of a light scattering medium and also at its upper and lower boundaries for the case of a homogeneous isotropic symmetric turbid medium illuminated by the monodirectional unpolarized wide light beam. The accuracy of the code was checked against benchmark results of Siewert (2000). Five first digits in our calculations coincide with that given by Siewert (2000). For some rare cases, we found the difference in the sixth digit (not more than 1–2 units). This confirms a high accuracy of the DOT implementation in the SCIAPOL\_1.0.

To demonstrate the capabilities of the code, we consider now several physical problems. The first one is related to the molecular scattering in the terrestrial atmosphere.

### 3. Results of numerical calculations

#### 3.1. Molecular scattering

We start the application of our code from the case of molecular scattering. This problem is the most extensively studied among all other vector transport problems. Both analytical results (Chandrasekhar, 1950; Sobolev, 1956; van de Hulst, 1980) and extensive tables (Coulson et al., 1960) are available both for intensity and polarization characteristics of light reflected and transmitted by a molecular atmosphere.

It should be noted that remote sensing of aerosols and clouds from space requires a subtraction of the molecular scattering signal from the total measured radiance. This is done using so-called pre-calculated look-up-tables (LUTs) of the Rayleigh intensity depending on the ground elevation, solar and viewing angles, the relative azimuths between the Sun and receiver positions, and sensing wavelengths (Hsu et al., 2004). Mishchenko et al. (1994) clearly showed that the VRTE (and not the SRTE) should be used in the construction of LUTs. This is also confirmed by Fig. 1 generated using our code. This figure shows the dependence of the relative error of the scalar approximation  $\varepsilon$  in percent as the function of the optical thickness of the molecular atmosphere at the nadir observation conditions, several solar angles and  $\omega_0=1$ . The value of the error is defined as:  $\varepsilon=100(I-I_s/I_v)$ , where  $I_s$  is the intensity obtained from the solution of the scalar problem and  $I_v$  is the intensity of the reflected light obtained using the VRTE. We see that the error  $\varepsilon$  could be quite large especially for the nadir illumination and grazing incidence angles at  $\vartheta=0^\circ$ . The error has a maximum around the optical thickness 1, which roughly corresponds to the wavelength 320 nm in the case of the terrestrial atmosphere (Bucholtz, 1995). Note that wavelengths  $\lambda<320$  nm ( $\tau>1$ ) are not extensively used for lower atmosphere remote sensing due to the interference of generally unknown ozone absorption. Generally, the error of the scalar approximation can be neglected for  $\tau<0.02$ , which corresponds to the wavelengths  $\lambda\geq 800$  nm. So the scalar approximation can be used in the construction of LUTs in the near-infrared. However, this is not the case in the visible and especially in the UV-region of the electromagnetic spectrum. This fact is

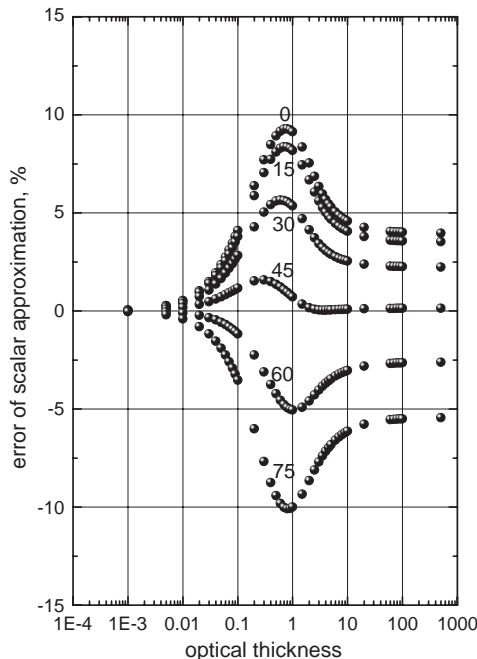


Fig. 1. Dependence of the scalar approximation error on the molecular optical thickness at nadir observation conditions for solar zenith angles 0, 15, 30, 45, 60, and 75°.

ignored in some modern aerosol retrieval techniques, which leads to the increased errors of retrievals depending on the wavelength used and the illumination/observation conditions of the scene under study.

It is known that the intensity of the singly scattered light does not differ in both scalar and vector formulations under unpolarized light illumination conditions. Hence, we have  $\varepsilon \rightarrow 0$  as  $\tau \rightarrow 0$ . The intensity of reflected light for semi-infinite media only weakly depends on the vector nature of light fields. This is due to the randomization of light polarization states by multiple light scattering. Therefore, one could expect the existence of the maxima of the absolute error somewhere in the transition zone from single scattering regime to highly developed multiple light scattering. Such maxima are clearly visible in our calculations presented in Fig. 1 at  $0.2 \leq \tau \leq 1$ .

It is interesting to see that the scalar approximation can either overestimate the reflected light intensity (e.g., for the solar zenith angles 0–45° and the nadir observation) or underestimate the reflected light intensity (e.g., for the solar zenith angles larger than 45° and the nadir observation, see Fig. 1). To understand this feature better, we plotted the value of  $\varepsilon$  as the function of the scattering angle  $\theta$  in Fig. 2. The scattering angle is defined as:

$$\theta = \arccos(-\mu\mu_0 + ss_0\cos\phi), \tag{26}$$

where  $s = \sqrt{1 - \mu^2}$ ,  $s_0 = \sqrt{1 - \mu_0^2}$ . In particular, it follows at  $\mu=1$  as used in Fig. 2:  $\theta = \pi - \vartheta_0$ . It follows from Fig. 2 that the error of the scalar approximation (at  $\varepsilon > 0$ ) is the largest at  $\theta = \pi$ . This coincides with the findings shown in Fig. 1 because the case of the solar zenith angle equal to zero at the nadir observation corresponds to the exact backscattering geometry (see the upper curve in Fig. 1). It is known that the scalar and vector theory produce the same results for the single scattering under unpolarized solar light illumination conditions. However, this is not the case for the secondary scattering and generally for multiple light scattering regime. The largest differences should occur at scattering angles close to 90° because then the degree of polarization of singly scattered light is close to 100% for molecular scattering.

We have approximately for the upper-left 2\*2 sub-matrix of the general Stokes matrix for molecular scattering at the scattering angle 90° (Kokhanovsky, 2003):

$$\hat{C} = \begin{pmatrix} 1 & 1 \\ 1 & 1 \end{pmatrix}, \tag{27}$$

where we neglected the constant multiplier. This matrix produces the following reduced Stokes vector  $\vec{s}$  of the singly scattered light at  $\theta=90^\circ$  for the incident unpolarized light:

$$\vec{s} = \begin{pmatrix} 1 \\ 1 \end{pmatrix}. \tag{28}$$

We define the reduced vector  $\vec{s}$  as the Stokes vector  $\vec{S}$  with neglected components  $U, V$ . Clearly, it follows for the double scattering in the same plane as for the incident light:

$$\vec{s} = \begin{pmatrix} 2 \\ 2 \end{pmatrix}. \tag{29}$$

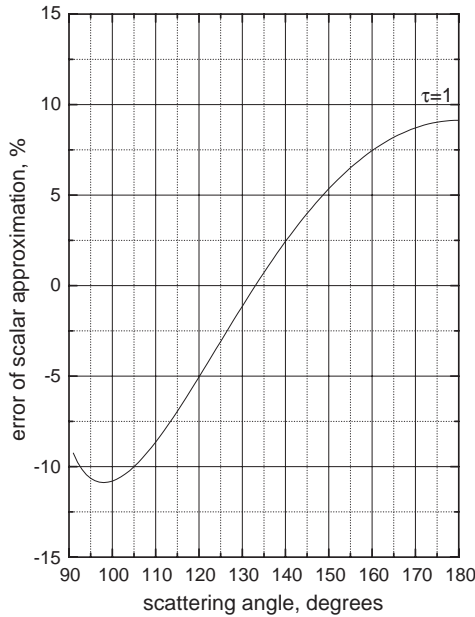


Fig. 2. Dependence of the scalar approximation error on the scattering angle at the optical thickness 1 for the molecular atmosphere. Calculations were performed at nadir observation conditions and  $\vartheta=0^\circ$  ( $1^\circ$ )  $89^\circ$ .

We have, however, for the double scalar scattering (both scatterings are at right angles and in the same scattering plane):

$$\vec{s} = \begin{pmatrix} 1 \\ 0 \end{pmatrix}. \quad (30)$$

So the intensity of scattered light is two times smaller for the secondary scattering in the scalar approximation as compared to the case, where the vector character of scattering is fully accounted for. This explains the large positive errors in the intensity of reflected light for the backscattering geometry as shown in Fig. 1 ( $I_s < I_v$ ). This physical insight is due to Mishchenko et al. (1994), who also explained the minimum for the negative  $\varepsilon$  (see Fig. 1) using similar arguments as given above for 2 scatterings at right angles to each other but with the rotation of the scattering plane by  $90^\circ$  for the second scattering. This gives for the intensity of scattered light:  $I_v=0$  The normalized intensity  $I_s$  is still equal to 1 for the scalar case. This explains the overestimation of the reflected light intensity at  $\vartheta_0=75^\circ$  by the SRTE in Fig. 1 (see also Fig. 2). Then the scattering angle is  $105^\circ$ , which is pretty close to  $90^\circ$ . Note that the minimum in Fig. 2 occurs at  $\theta=97^\circ$  and not at exactly  $90^\circ$  due to the influence of triple and higher order scatterings.

The optical thickness of molecular atmosphere for wavelengths usually used for the tropospheric remote sensing ( $\lambda > 320$  nm) is smaller than 1.0. So it is of importance to see if the single scattering approximation (SSA) can be used to find the Stokes vector of

scattered light for molecular atmosphere in this case. The SSA is written in the following form (Hansen and Travis, 1974):

$$\vec{\mathfrak{R}} = \frac{\omega_0 \hat{P}(\mu, \mu_0, \varphi)}{4(\mu + \mu_0)} \{1 - \exp(-m\tau)\} \vec{J}, \tag{31}$$

where  $\omega_0$  is the single scattering albedo assumed to be equal 1.0 in this study,  $m = (\mu^{-1} + \mu_0^{-1})$  and

$$\vec{F} = F_0 \vec{J}, \quad \vec{J} = \begin{pmatrix} 1 \\ 0 \\ 0 \\ 0 \end{pmatrix}, \tag{32}$$

assuming unpolarized light illumination conditions.

The components of the normalized Stokes vector of the reflected light  $\vec{\mathfrak{R}}$  are defined as follows:

$$\mathfrak{R}_1 = \pi I_r / F_0 \mu_0, \quad \mathfrak{R}_2 = \pi Q_r / F_0 \mu_0, \quad \mathfrak{R}_3 = \pi U_r / F_0 \mu_0, \quad \mathfrak{R}_4 = \pi V_r / F_0 \mu_0, \tag{33}$$

where the Stokes vector of reflected light is given as

$$\vec{S}_r = \begin{pmatrix} I_r \\ Q_r \\ U_r \\ V_r \end{pmatrix}. \tag{34}$$

We present results of calculations using Eq. (31) for the reflection function  $R \equiv \mathfrak{R}_1$  and the polarization difference  $D = -\mathfrak{R}_2$  in Fig. 3. The phase matrix of the Rayleigh scattering in the form (Kokhanovsky, 2003):

$$\hat{P}(\theta) = \frac{3}{4} \begin{pmatrix} 1 + \cos^2\theta & -\sin^2\theta & 0 & 0 \\ -\sin^2\theta & 1 + \cos^2\theta & 0 & 0 \\ 0 & 0 & 2\cos\theta & 0 \\ 0 & 0 & 0 & 2\cos\theta \end{pmatrix} \tag{35}$$

was used in approximate calculations. Greek symbols as shown in Eq. (8) were used in exact calculations with SCIAPOL. Note that we neglect here possible depolarization effects, which exist due to the molecular anisotropy.

We see that SSA underestimates both  $R$  and  $D$  and can be used with accuracy better than 5% only at  $\tau \leq 0.05$  (or for wavelengths larger than approximately 650 nm (Bucholtz, 1995)). So the most of visible and UV parts of the electromagnetic spectrum are not covered by this approximation for molecular scattering in the terrestrial atmosphere. However, Fig. 3 shows that the dependence of the error  $\Delta = 100(1 - R_{SSA}/R_v)$  on the solar angle is not very pronounced. So we can introduce a correction multiplier  $f(\tau)$  to Eq. (31) at the average angle  $45^\circ$ . Then we have:

$$R = R_{ss} f(\tau), \quad D = S_{ss} \psi(\tau) \tag{36}$$

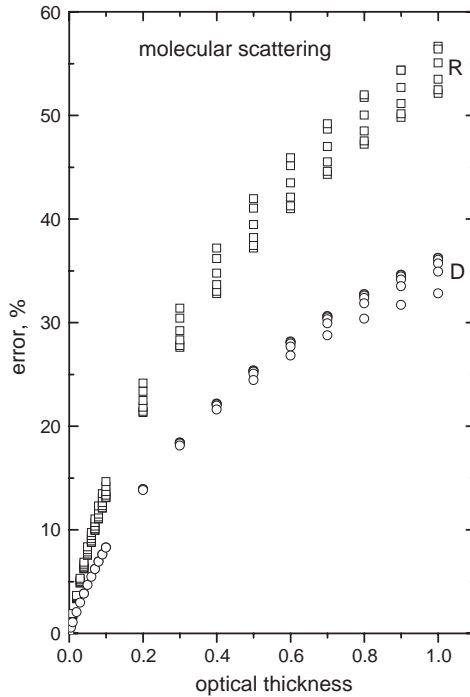


Fig. 3. Dependence of the error of the single scattering approximation on the molecular optical thickness for the reflection function  $R$  and the polarization difference  $D$ . The spread in the vertical direction is due to different solar zenith angles at the nadir observation.

where we found using the parameterization of numerical results that

$$f(\tau) = 1 + \frac{(7 - \tau)\tau}{5}, \quad \psi(\tau) = 1 + a\tau - b\tau^2 + c\tau^3 \quad (37)$$

and  $a=0.864$ ,  $b=0.442$ ,  $c=0.133$ . The accuracy of this approximation at  $\vartheta=0^\circ$  is given in Fig. 4 both for  $R$  and  $D$ . We see that the accuracy is much more improved in comparison with Fig. 3. The error is smaller than 5% for most solar illumination conditions and  $\tau \leq 1$ , which corresponds approximately to the wavelengths  $\lambda \geq 320$  nm in the case of the terrestrial atmosphere (Bucholtz, 1995). Similar results can be obtained for other observation conditions as well. Also they can be improved, if necessary, to cover still larger values of  $\tau$ . We leave this problem at this point, however, and bring the attention to the case of a cloudy atmosphere.

### 3.2. Clouds

The calculations for the case of a cloudy atmosphere take much more computer time as compared to the molecular scattering. This is not related to the larger optical thickness of clouds, which can reach 100 and more, but solely due to the peaked phase

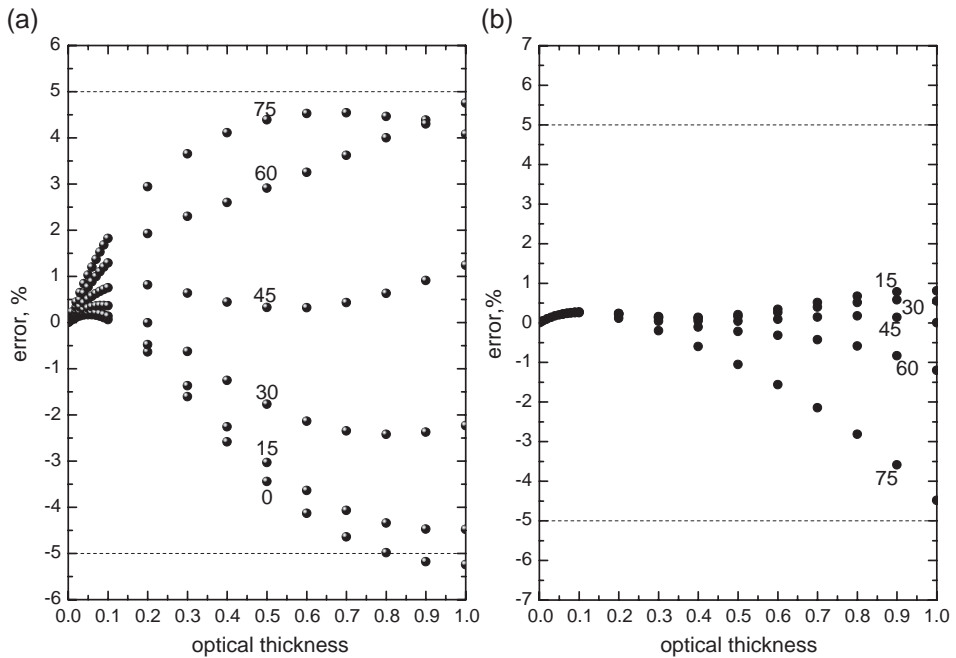


Fig. 4. (a) Dependence of the error of the modified single scattering approximation for the reflectance  $R$  given by Eq. (37) on the molecular optical thickness for solar zenith angles 0, 15, 30, 45, 60, and 75° at nadir observation. (b) The same as in panel (a) except for  $D$ .

functions of water clouds. This means that one must account for a lot of Legendre polynomials in the correspondent expansions (e.g., large values of  $L$  in Eq. (2)). This also leads to a large number  $N$  of gaussian quadrature points required to solve this problem ( $N \approx L/2$ ). This obstacle can be avoided using a so-called delta- $M$  approximation (Nakajima and Tanaka, 1988; Min and Duan, 2004). However, this option is not implemented in the code. So results presented here do not contain any approximations whatsoever.

We show the cloud reflection function calculated using our code in Fig. 5. As one might expect, the reflection function increases with  $\tau$ . It reaches an asymptotic value for a semi-infinite cloud at  $\tau \approx 11$  for the wavelength 2130 nm. For a nonabsorbing wavelength the asymptotic value is reached at much higher values of  $\tau$  ( $\tau \sim 500$  at the wavelength 865 nm, see Fig. 5). The single scattering approximation works quite well for  $\tau \approx 0.03$  and below. So it can be used for estimation of scattering characteristics of subvisual Cirrus but not for most of water and ice clouds present in troposphere. Performance of the SSA for the polarization difference  $D$  is much better. It is valid at least up to  $\tau = 0.1$  (and even up to  $\tau = 1.0$  for the wavelength  $\lambda = 2130$  nm, see Fig. 6).

There is a peculiarity in the behavior of the function  $D(\tau)$  at  $\lambda = 2130$  nm shown in Fig. 6. In particular, there is a maximum around  $\tau = 1$ . Such maxima are not particularly pronounced for other solar angles shown in Fig. 7. The existence of the maximum cannot be explained on physical grounds because the difference  $D$  does not have a direct

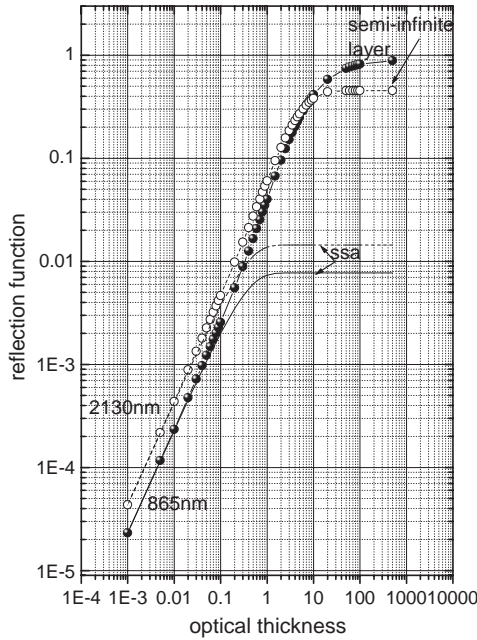


Fig. 5. Dependence of the cloud reflection function on the cloud optical thickness at wavelengths 865 and 2130 nm. The results for the semi-infinite layer and the single scattering approximation are also shown. The solar zenith angle is  $60^\circ$ . The observation zenith angle is  $0^\circ$ . The phase function was calculated using Mie theory for the Deirmendjian’s Cloud C1 model (Deirmendjian, 1969). The effective radius of droplets  $a_{ef}$  is equal to  $6 \mu\text{m}$  in the framework of the Cloud C1 model.

physical meaning. Physically based quantities  $I_l$ ,  $I_r$ ,  $R$ , and also the degree of polarization

$$P = \frac{D}{R} \tag{38}$$

all behave in the monotonous way (see, e.g., Fig. 8).

Yet another peculiarity of the function  $D(\tau)$  shown in Figs. 6 and 7 is that it reaches its asymptotical value for a semi-infinite cloud  $D_\infty$  at relatively small values of  $\tau = \tau_\infty$  ( $\tau_\infty = 3\text{--}10$ , depending on the wavelength, see Fig. 6), which is not the case for  $R$  and  $P$  (see Fig. 8). The optical thickness of water clouds is usually larger than  $\tau_\infty$ . It means that the value of  $D$  is a priori known for a given wavelength and the effective radius of droplets. Such a peculiarity can be used to estimate the sub-pixel cloud fraction  $\mathbf{K}$  from remote sensing measurements. Indeed, the values of  $R$  and  $D$  can be presented as

$$R = \mathbf{K}R_c + (1 - \mathbf{K})R_a, \quad D = \mathbf{K}D_c + (1 - \mathbf{K})D_a \tag{39}$$

for a partially cloudy scene, where the symbol  $c$  shows that the correspondent characteristic is related to the cloudy portion of the pixel and  $a$  denotes the characteristic of a cloudless atmosphere. It is known that values of  $R_a$  and  $D_a$  are determined mostly by the molecular scattering in the UV-region of the electromagnetic spectrum ( $R_a \rightarrow R_m$ ,  $D_a \rightarrow D_m$ , where  $m$  denotes the pure molecular scattering case (no clouds and aerosols)).

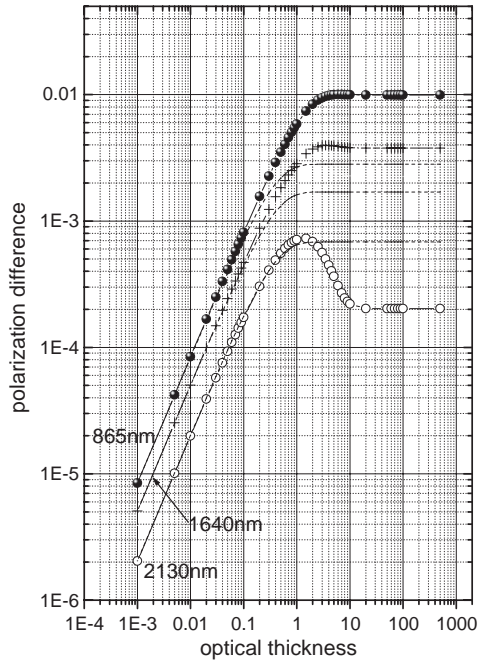


Fig. 6. Dependence of the polarization difference  $D$  on the cloud optical thickness at wavelengths 865, 1640, and 2130 nm. The results for the semi-infinite layer and the single scattering approximation are also shown. The solar zenith angle is  $60^\circ$ . The observation zenith angle is  $0^\circ$ . The phase function was calculated using Mie theory for the Deirmendjian’s Cloud C1 model. Exact results are given by symbols.

This contribution is known a priori due to the relative stability of the Rayleigh optical thickness for a given wavelength. Then it follows in the UV:

$$\mathbf{K} = \frac{D - D_m}{D_\infty - D_m}, R_c = \mathbf{K}^{-1}R - (\mathbf{K}^{-1} - 1)R_m, \tag{40}$$

which allows us to find not only  $\mathbf{K}$  but also the cloud optical thickness in a partially cloudy scene, e.g., using the following relationship between  $R_c$  and  $\tau$  valid at  $\tau \geq 5$  in the UV (Nakajima and King, 1992; Kokhanovsky, 2003, 2004a):

$$R_c(\mu, \mu_0, \phi) = R_\infty(\mu, \mu_0, \phi) - t(\tau)K_0(\mu_0)K_0(\mu), \tag{41}$$

where

$$t(\tau) = \frac{1}{1.07 + 0.75(1 - g)\tau}, \tag{42}$$

and  $g \approx 0.85$  for water droplets. Analytical expressions for functions  $R_\infty(\mu, \mu_0, \phi)$  and  $K_0(\mu)$  are given in the Appendix A.

The value of  $D_\infty$  depends on the effective radius of droplets  $a_{ef}$  defined as the ratio of the third-to-second moment of the particle size distribution. Therefore,  $D_\infty$  is not known a priori. So one should assume the most frequently appearing radius of droplets (e.g.,

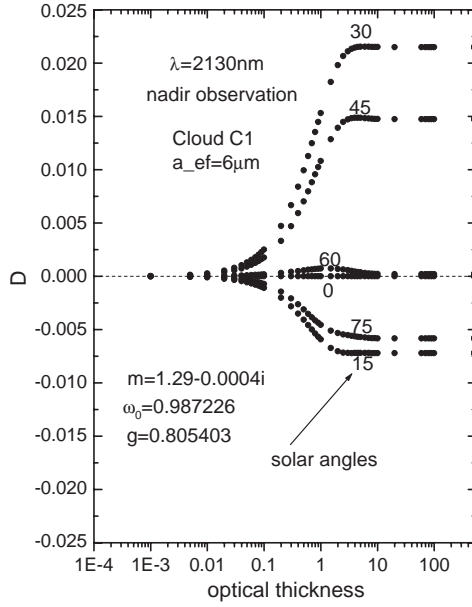


Fig. 7. The same as in Fig. 6 but for various solar zenith angles at the wavelength 2130 nm. The refractive index used in calculations of the phase function using Mie theory for the Deirmendjian’s Cloud C1 model is also shown. Values of  $\omega_0$  and  $g$  give correspondent values of the single scattering albedo and the asymmetry parameter.

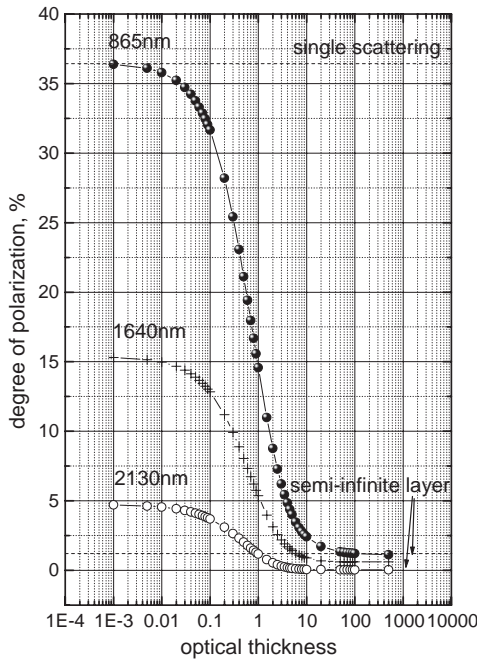


Fig. 8. The same as in Fig. 6 but for the degree of polarization in percent.

$a_{ef}=10 \mu\text{m}$ ) or use the viewing observation geometry where the dependence of  $D_\infty$  on  $a_{ef}$  is weak. Another interesting possibility arises at geometries, where  $D_c=0$  (and, therefore,  $\mathbf{P}=0$ , see Fig. 9). Then it follows from Eq. (39):  $\mathbf{K}=1-DD_m^{-1}$ . So if the measured value of  $D$  is equal to  $D_m$ , then we have  $\mathbf{K}=0$  at this particular geometry.  $\mathbf{K}$  is equal to one for a completely cloudy atmosphere ( $D=0$  for clouds at the chosen favorable geometry). It follows from Fig. 9 that  $D_c \approx 0$  at the solar angle  $22^\circ$  and the nadir observation. This corresponds to the scattering angle  $158^\circ$ . So if one constructs the device capable to measure  $D$  at this scattering angle, he will be able to determine the cloud fraction  $\mathbf{K}$  quite accurately. The origin of minimum at  $\theta=158^\circ$  is due to peculiarities of single scattering by water droplets. Note that multiple scattering hardly moves the positions, where the degree of polarization of singly scattered light vanishes (Kokhanovsky, 2003).

Let us consider the degree of polarization of light reflected from clouds. This is shown in Fig. 8 for several wavelengths. We see that  $\mathbf{P}$  decreases with the optical thickness for all wavelengths. This is due to increased multiple light scattering, which also increases the entropy and depolarizes light field. One can easily derive the following approximation for cloudy media:

$$\mathbf{P} = \frac{\mathbf{P}_\infty}{1 - ut}, \tag{43}$$

where we suppressed arguments and  $u=K_0(\mu)K_0(\mu_0)/R_\infty(\mu,\mu_0,\phi)$ ,  $\mathbf{P}_\infty=D_\infty(\mu,\mu_0,\phi)/R_\infty(\mu,\mu_0,\phi)$ . Eq. (43) is obtained from Eqs. (38), (41), taking into account the weak

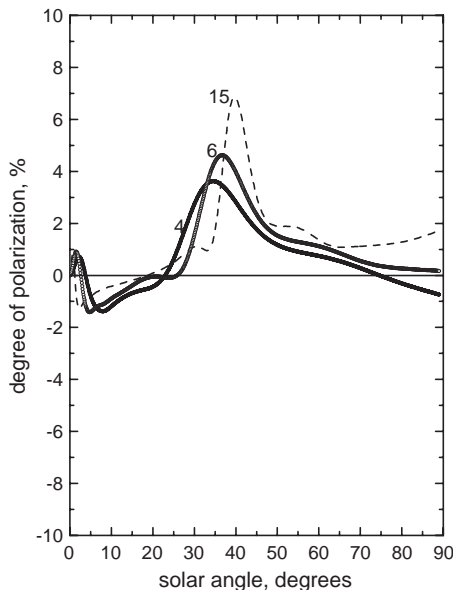


Fig. 9. Dependence of the degree of polarization  $\mathbf{P}$  on the solar zenith angle at the optical thickness 500, nadir observation, and several effective radii of droplets. The phase function was calculated using Mie theory for the gamma particle size distribution with the half-width, which is equal to that for the Deirmendjian's Cloud C1 model but with different effective radii  $a_{ef}=4, 6,$  and  $15 \mu\text{m}$  at the wavelength 865 nm.

sensitivity of  $D$  to the value of  $\tau$ . The accuracy of this approximation is shown in Fig. 10. We find that the error is smaller than 5% at  $\tau \geq 5$ . Therefore, Eq. (43) reduces the calculation of the degree of polarization of reflected light to the derivation of  $\mathbf{P}_\infty$ . This function can be taken from correspondent LUTs. Also parameterizations can be used (see, e.g., Kokhanovsky and Weichert, 2002). Note that Eq. (43) is much more simpler then the exact asymptotical results valid as  $\tau \rightarrow \infty$  (Domke, 1978a,b).

### 3.3. Aerosols

The calculations for aerosols are simpler than those for clouds because the aerosol optical thickness (AOT) is rarely exceeds 1.0 with average values around 0.1–0.2 in the visible (Ignatov and Stowe, 2002). Also the phase functions of aerosols are not so peaked as in the case of cloudy media (d’Almeida et al., 1991). This speeds computer calculations considerably.

Note that the reflected light intensity for aerosols calculated in the scalar approximation can be biased in comparison with exact vector results for aerosol with small values of  $a_{ef}$  and/or large wavelengths (see Fig. 11). This means that correspondent LUTs should be calculated using the VRTE (Hsu et al., 2004). However, there is no problem with clouds in this respect. Clouds droplets generally have radii above  $1 \mu\text{m}$ . Then the error of the scalar approximation is well below 1% (see Fig. 11).

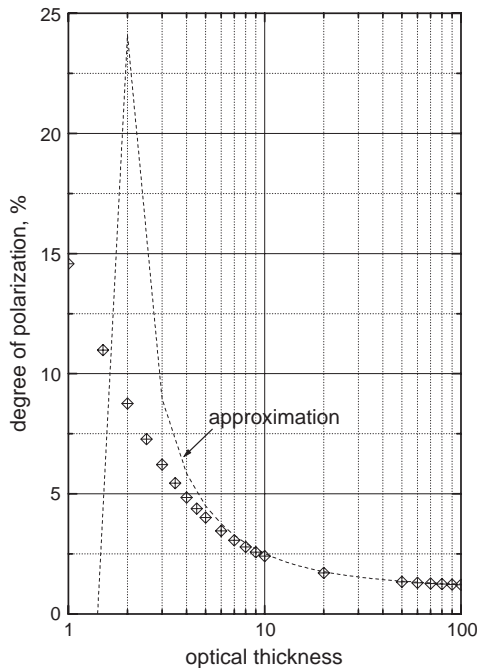


Fig. 10. Dependence of the degree of polarization  $\mathbf{P}$  on the optical thickness as obtained using Eq. (43) (dashed line) and exact radiative transfer calculations (symbols) at  $\vartheta_0=0^\circ$ ,  $\vartheta=60^\circ$ ,  $\lambda=865 \text{ nm}$  for the Deirmendjian's Cloud C1 model.

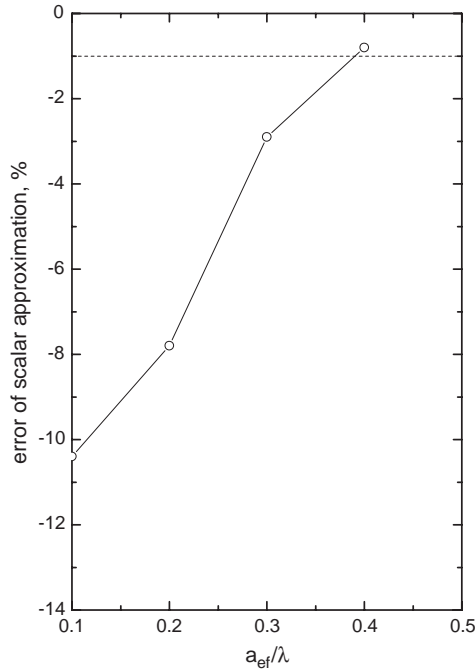


Fig. 11. Dependence of the scalar approximation error  $\varepsilon$  on the ratio  $a_{\text{eff}}/\lambda$ . Results were obtained using the gamma size distribution of water droplets with the coefficient of variance 38% at  $\vartheta_0=0^\circ$ ,  $\vartheta=60^\circ$ ,  $\lambda=500$  nm for effective radii 0.05, 0.1, 0.15, and 0.2  $\mu\text{m}$ . These results show that the SRTE can be used to calculate the intensity of reflected light for  $x_{\text{eff}}>2$  in the case under consideration. For smaller values of the effective size parameter  $x_{\text{eff}}=2\pi a_{\text{eff}}/\lambda$ , the VRTE should be used.

We show the dependence of the reflection function and the degree of polarization of light reflected from the aerosol media with refractive indices  $1.43 - i\chi$  and  $1.53 - i\chi$ , where  $\chi=0.006$  in Figs. 12 and 13. It was assumed that the particle size distribution is given by

$$f(a) = Aa^v \exp\left(-v \frac{a}{a_0}\right) \tag{44}$$

with  $A=v^{v+1}a_0^{-v-1}\Gamma^{-1}(v+1)$ ,  $v=6$ ,  $a_0=400$  nm. The calculations are performed using Mie theory (Van de Hulst, 1957) at the wavelength 550 nm. It follows that both  $R$  and  $D$  depend on the value of the refractive index  $n$  of particles. On one hand, it means that the value of  $n$  can be retrieved from reflected light measurements. On the other hand, we need to give much more attention to studies of the refractive index of terrestrial aerosols. Without advances in this area, LUTs used in the aerosol retrieval algorithms, which are based on averaged values of the aerosol refractive index, can give considerably biased results. Indeed, it follows from Fig. 12 that the reflectances are lower at the refractive index  $n=1.43$  as compared to the case  $n=1.53$ . Therefore, if the refractive index 1.53 is assumed in the construction of correspondent LUTs for particles with lower  $n$  (e.g., due to uptake of water), then the retrieved AOT will be underestimated. The error will be even larger if the degree of

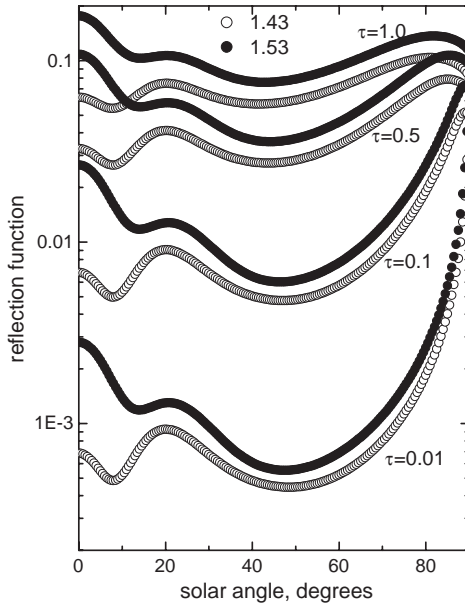


Fig. 12. Dependence of the reflection function on the solar zenith angle at nadir observation for optical thicknesses 0.01, 0.1, 0.5, 1.0, and the refractive indices  $n=1.43, 1.53$ . The particle size distribution and the aerosol absorption coefficient  $\chi$  are given the text.

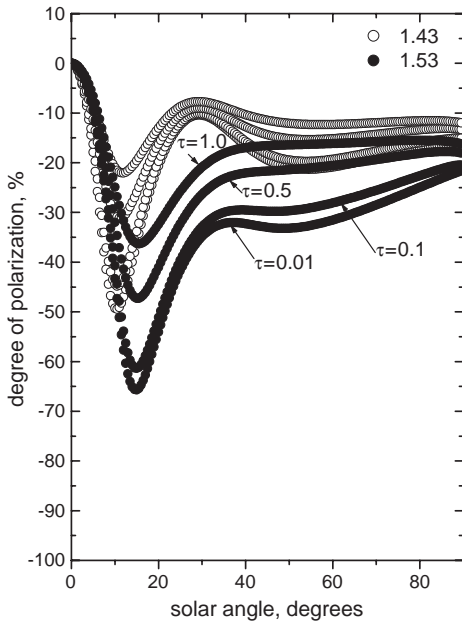


Fig. 13. The same as in Fig. 12 except for the degree of polarization.

polarization measurements are used assuming a wrong  $n$  (see Fig. 13). It also means that the refractive index of particles should be retrieved simultaneously with the AOT to avoid such biases. Correspondent retrieval algorithms have already been developed (Zhao et al., 1997). Considerable efforts should be put in their further development and application to satellite data. For this, however, one needs data from optical instruments capable to measure both polarization and intensity of reflected light (Deschamps et al., 1994). The possibility to change the viewing conditions for the same ground target (see, e. g., Moroney et al., 2002, and references therein) is also of a great importance for this task. The general behavior of curves  $\mathbf{P}(\vartheta_0)$  is quite different for different refractive indices (Zhao et al., 1997). This can be also used to find  $n$  and constrain correspondent LUTs.

An interesting feature of the degree of polarization shown in Fig. 13 is that it is negative for almost all solar angles. This is due to the correspondent behavior of the degree of polarization for singly scattered light in the case studied (see Fig. 14), which is negative or partially linearly polarized in the direction parallel to the meridional plane for all scattering angles. This is in contrast with molecular and cloud scattering (see Fig. 14). We see that the measurements of sign and angular dependence of  $\mathbf{P}$  is of a great importance for the atmospheric remote sensing. To understand such measurements, advanced radiative transfer codes are needed. One of them is presented here.

It must be underlined that molecular and cloud scattering results given in Fig. 14 capture main characteristics of the angular dependence of the degree of polarization of

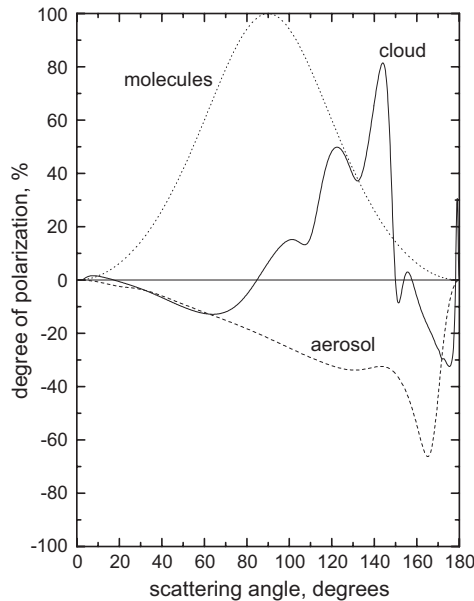


Fig. 14. Dependence of the degree of polarization on the scattering angle  $\theta$  for single light scattering of unpolarized radiation by molecules, cloud droplets, and the aerosol medium described in the text calculated using Mie theory at the wavelength 550 nm. Water droplets have the effective radius  $6 \mu\text{m}$  and the refractive index 1.333. Aerosol particles have the effective radius  $0.6 \mu\text{m}$  and the refractive index  $1.53-0.006i$ . Particle size distributions are given by Eq. (44).

light scattered by these constituents in nature. This is not the case for the aerosol medium example given here. Properties of aerosol media vary considerably depending on the chemical composition of aerosol particles, their morphology, the shape of particles, and their size (Junge, 1963). In particular, aerosols can exhibit a Rayleigh-type polarization signature (however, reduced in the magnitude (Volten, 2001)). Therefore, aerosols present much more challenging task for a modeler.

#### 4. Conclusions

We have developed a new vector radiative transfer code based on the discrete-ordinates technique as described by Siewert (2000). The code is freely accessible via INTERNET at [www.iup.physik.uni-bremen.de/~alexk](http://www.iup.physik.uni-bremen.de/~alexk). We applied the code to the solution of selected physical problems and developed new approximations for calculations of reflectances and degrees of polarization of reflected light for thick clouds and thin molecular atmospheres.

All these questions were considered for the case of a vertically homogeneous plane-parallel slab illuminated from above by a monodirectional wide unpolarized light beam. In reality, however, clouds, aerosols, and molecules of various gases exist in the atmosphere simultaneously. Also their characteristics change with height. Therefore, there is a need to extend the SCIAPOL to the case of vertically inhomogeneous media. This will be a subject of our next work publication.

#### Acknowledgements

Parts of this work have been funded by the German Science Foundation DFG (grant BU 688/8-1), the German Ministry of Education and Research BMBF (grant 07UFE12/8) and the German Aerospace Centre DLR (grant 50EE0027).

#### Appendix A. Auxiliary functions

Auxiliary functions are given by the following equations (Kokhanovsky, 2004a,b):

$$K_0(\xi) = \frac{3}{7} [1 + 2\xi],$$

$$R(\xi, \eta, \varphi) = \frac{A + B(\xi + \eta) + C\xi\eta + F(\theta)}{4(\xi + \eta)},$$

where  $F(\theta) = p(\theta) - \bar{p}(\theta)$ ,  $A \approx 3.944$ ,  $B \approx -2.5$ ,  $C \approx 10.664$ ,  $p(\theta)$  is the phase function, and  $\bar{p}(\theta)$  is the azimuthally averaged phase function under study. Further details and study of accuracy of these approximations are given by Kokhanovsky (2004a,b).

## Appendix B. The particular solution of the differential equation

In this Appendix, we describe briefly some details, which are implemented in our vector code to calculate the infinite medium Green functions and the particular solution.

We start from the general equation for the eigenvalue problem:

$$FEX_r = \lambda X_r,$$

where matrices  $F$  and  $E$  are defined according to Eq. (36) in the paper by Siewert (2000),  $\lambda$  is the eigenvalue, and  $X_r$  is the right eigenvector.

If eigenvalues  $\lambda_j$  and eigenvectors  $X_r(\lambda_j)$  are found, the separation constants occur in plus/minus pairs. Let  $v_j$  for  $j=1, 2, \dots, 4N$  denote the reciprocal of the square root of  $\lambda_j$ . Then we obtain an elementary solution of a homogeneous equation:

$$\vec{\Phi}_{\pm}(v_j) = \frac{1}{2} M^{-1} [I \pm v_j E] X_r(\lambda_j),$$

where  $I$  is the  $4N \times 4N$  unity matrix. To find adjoint vectors  $\vec{\Psi}_{\pm}(v_j)$  which are needed for calculations of the infinite medium Green function and a particular solution, we use the left eigenvectors of the matrix  $FE$ :

$$\vec{\Psi}_{\pm}(v_j) = \frac{1}{2} W^{-1} [v_j F^T \pm I] X_l(\lambda_j),$$

where “ $T$ ” denotes the transpose matrix,  $X_l(\lambda_j)$  is the left eigenvector.

Taking into account equations given above, we can simplify the calculation of the constant  $N(v_j)$  (see Eq. (64) given by Siewert, 2000):

$$N(v_j) = \vec{\Psi}_+^T(v_j) W M \vec{\Phi}_+(v_j) - \vec{\Psi}_-^T(v_j) W M \vec{\Phi}_-(v_j).$$

Inserting in this equation expressions for  $\vec{\Phi}_{\pm}(v_j)$  and  $\vec{\Psi}_{\pm}(v_j)$ , given above, we have:

$$N(v_j) = X_l^T(v_j) X_r(v_j).$$

We have used the subroutine DGEEV from the LAPACK package to compute the left and right eigenvectors of the matrix  $FE$ . The complex arithmetic is used in the code only for variables which contain complex separation constants. Otherwise, real arithmetic is used.

## References

- Anderson, E., Bai, Z., Bischof, C., Demmel, J., Dongarra, J., Du Croz, J., Greenbaum, A., Hammarling, S., McKenney, A., Ostrouchov, S., Sorenson, D., 1995. LAPACK. User’s Guide, 2nd ed. SIAM, Philadelphia.
- Bovensmann, H., et al., 1999. SCIAMACHY: mission objectives and measurement modes. *J. Atmos. Sci.* 56, 127–150.
- Bucholtz, A., 1995. Rayleigh-scattering calculations for the terrestrial atmosphere. *Appl. Opt.* 34, 2765–2773.
- Chandrasekhar, S., 1950. Radiative Transfer. Oxford Press, Oxford.
- Coulson, K.L., Dave, J.V., Sekera, Z., 1960. Tables Related to Radiation Emerging from a Planetary Atmosphere with Rayleigh Scattering. University of California Press, Berkeley.

- d'Almeida, G.A., et al., 1991. *Atmospheric Aerosols: Global Climatology and Radiative Characteristics*. A. Deepak Publ., New York.
- de Haan, J.F., 1987. Effects of aerosols on the brightness and polarization of cloudless planetary atmospheres. PhD thesis, Free University of Amsterdam.
- Deirmendjian, A., 1969. *Electromagnetic Scattering on Spherical Polydispersions*. Elsevier, Amsterdam.
- de Rooij, W.A., 1985. Reflection and transmission of polarized light by planetary atmospheres. PhD thesis, Free University of Amsterdam.
- Deschamps, P.-Y., et al., 1994. The POLDER Mission: instrument characteristics and scientific objectives. *IEEE Trans., GE* 32, 598–614.
- Domke, H., 1978a. Linear Fredholm integral equations for radiative transfer problems in finite plane-parallel media: I. Imbedding in an infinite medium. *Astron. Nachr.* 299, 87–93.
- Domke, H., 1978b. Linear Fredholm integral equations for radiative transfer problems in finite plane-parallel media: II. Imbedding in a semi-infinite medium. *Astron. Nachr.* 299, 95–102.
- Goloub, P., et al., 2000. Cloud thermodynamical phase classification from the POLDER spaceborne instrument. *J. Geophys. Res.*, D 105, 14747–14759.
- Hansen, J.E., Hovenier, J., 1974. Interpretation of the polarization of Venus. *J. Atmos. Sci.* 31, 1137–1160.
- Hansen, J.E., Travis, L.D., 1974. Light scattering in planetary atmospheres. *Space Sci. Rev.* 16, 527–610.
- Hovenier, J.W., 1971. Multiple scattering of polarized light in planetary atmospheres. *Astron. Astrophys.* 13, 7–29.
- Hsu, N.C., et al., 2004. Aerosol properties over bright-reflecting source regions. *IEEE Trans. Geosci. Remote Sens.* 42, 557–569.
- Ignatov, A., Stowe, L., 2002. Aerosol retrievals from individual AVHRR channels: Part II. Quality control, probability distribution functions, information content, and consistency checks of retrievals. *J. Atmos. Sci.* 59, 335–362.
- Ishimoto, H., Masuda, K., 2002. A Monte Carlo approach for the calculation of polarized light: application to an incident narrow beam. *J. Quant. Spectrosc. Radiat. Transfer* 72, 467–483.
- Junge, C.E., 1963. *Air Chemistry and Radiochemistry*. Academic Press, N.Y.
- Kokhanovsky, A.A., 2003. *Polarization Optics of Random Media*. Springer-Praxis, Berlin.
- Kokhanovsky, A.A., 2004a. *Light Scattering Media Optics: Problems and Solutions*. Springer-Praxis, Berlin.
- Kokhanovsky, A.A., 2004b. Reflection of light from nonabsorbing semi-infinite cloudy media: a simple approximation. *J. Quant. Spectrosc. Radiat. Transfer* 85, 35–55.
- Kokhanovsky, A.A., Weichert, R., 2002. The determination of the droplet effective size and optical depth of cloudy media from polarimetric measurements. *Appl. Opt.* 41, 3650–3658.
- Kuik, F., de Haan, J.F., Hovenier, J.W., 1992. Benchmark results for single scattering by spheroids. *J. Quant. Spectrosc. Radiat. Transfer* 47, 477–489.
- Lacis, A.A., Chowdhary, J., Mishchenko, M.I., Cairns, B., 1998. Modeling of errors in diffuse-sky radiation: vector vs. scalar treatment. *Geophys. Res. Lett.*, 135–138.
- Min, Q., Duan, M., 2004. A successive order of scattering model for solving vector radiative transfer in the atmosphere. *J. Quant. Spectrosc. Radiat. Transfer* 87, 243–259.
- Mishchenko, M.I., 2002. Vector radiative transfer equation for arbitrarily shaped and arbitrarily oriented particles: a microphysical derivation from statistical electromagnetics. *Appl. Opt.* 41, 7114–7135.
- Mishchenko, M.I., Travis, L.D., 1997. Satellite retrieval of aerosol properties over the ocean using polarization as well as intensity of reflected sunlight. *J. Geophys. Res.* 102, 16989–17013.
- Mishchenko, M.I., Lacis, A.A., Travis, L.D., 1994. Errors induced by the neglect of polarization in radiance calculations for Rayleigh-scattering atmospheres. *J. Quant. Spectrosc. Radiat. Transfer* 51, 491–510.
- Mishchenko, M.I., Travis, L.D., Lacis, A.A., 2002. *Scattering, Absorption, and Emission of Light by Small Particles*. Cambridge University Press.
- Moroney, C.R., Davies, R., Muller, J.P., 2002. Operational retrieval of cloud-top heights using MISR data. *IEEE Trans. Geosci. Remote Sens.* 40, 1532–1546.
- Nakajima, T., King, M.D., 1992. Asymptotic theory for optically thick layers: application to the discrete ordinates method. *Appl. Opt.* 31, 7669–7683.
- Nakajima, T., Tanaka, M., 1988. Algorithms for radiative intensity calculations in moderately thick atmospheres using a truncation approximation. *J. Quant. Spectrosc. Radiat. Transfer* 40, 51–69.

- Rayleigh, Lord, 1871. On the light from the sky, its polarization and colour, *Philos. Mag.*, 41, 107–120, 274–279.
- Rozenberg, G.V., 1955. Stokes vector-parameter. *Usp. Fiz. Nauk* 56, 77–110.
- Siewert, C.E., 1997. On the phase matrix basic law to the scattering of polarized light. *Astron. Astrophys.* 109, 195–200.
- Siewert, C.E., 2000. A discrete-ordinates solution for radiative-transfer models that include polarization effects. *J. Quant. Spectrosc. Radiat. Transfer* 64, 227–254.
- Sobolev, V.V., 1956. *Radiative Transfer in Stellar and Planetary Atmospheres*. Gostekhizdat, Moscow.
- Tynes, H.H., Kattawar, G.W., Zege, E.P., Katsev, I.L., Prikhach, A.S., Chaikovskaya, L.I., 2001. Monte Carlo and multicomponent approximation methods for vector radiative transfer by use of effective Mueller matrix calculations. *Appl. Opt.* 40, 400–412.
- Van de Hulst, H.C., 1957. *Light Scattering by Small Particles*. Wiley, N.Y.
- van de Hulst, H.C., 1980. *Multiple Light Scattering: Tables, Formulas and Applications*. Academic Press, N.Y.
- Volten, H., 2001. *Light scattering by small planetary particles*, PhD thesis, Free University of Amsterdam.
- Zhao, F., Gong, Z., Hu, H., Tanaka, M., Hayasaka, T., 1997. Simultaneous determination of the aerosol complex index of refraction and size distribution from scattering measurements of polarized light. *Appl. Opt.* 36, 7992–8001.